

# Impacts of pure seawater absorption coefficient on remotely sensed inherent optical properties in oligotrophic waters

XIAOLONG YU,<sup>1,\*</sup>  ZHONGPING LEE,<sup>2</sup> JIANWEI WEI,<sup>2</sup> AND SHAOLING SHANG<sup>1</sup>

<sup>1</sup>State Key Laboratory of Marine Environmental Science, College of Ocean and Earth Sciences, Xiamen University, Xiamen 361101, China

<sup>2</sup>School for the Environment, University of Massachusetts Boston, Boston, MA 02125, USA

\*xlyu@xmu.edu.cn

**Abstract:** The spectral absorption coefficient of pure seawater ( $a_w(\lambda)$ ) in published studies differ significantly in the blue domain, yet the impacts of such discrepancies on the inherent optical properties (IOPs) derived from ocean color have been scarcely documented. In this study, we confirm that changes in  $a_w(\lambda)$  may have significant impacts on retrieved IOPs in oligotrophic waters, especially for the phytoplankton absorption coefficient ( $a_{ph}(\lambda)$ ). Two sets of  $a_w(\lambda)$  data,  $a_{w\_PF97}$  (Appl. Opt. 36, 8710, 1997) and  $a_{w\_Lee15}$  (Appl. Opt. 54, 546, 2015), were selected for optical inversion analysis. It is found that  $a_{ph}(\lambda)$  retrieved with  $a_{w\_Lee15}$  agree better with the *in-situ* measurements in oligotrophic waters. Further applications to satellite images show that the derived  $a_{ph}(\lambda)$  using  $a_{w\_Lee15}$  can be up to 238% higher than the retrievals using  $a_{w\_PF97}$  in the core zone of the subtropical ocean gyres. Given that  $a_{w\_PF97}$  is commonly accepted as the “standard”  $a_w(\lambda)$  by the ocean color community in the past decades, this study highlights the need and importance to update  $a_w(\lambda)$  with  $a_{w\_Lee15}$  for IOPs retrievals in oligotrophic waters.

© 2019 Optical Society of America under the terms of the [OSA Open Access Publishing Agreement](#)

## 1. Introduction

Water molecules, together with colored dissolved organic matter (CDOM) and particulate matter, are the optically important components in natural waters. The absorption and scattering properties of these components, known as the inherent optical properties (IOPs), determine the propagation of light within the water body [1]. In Case 1 waters, defined by Morel [2], pure seawater, phytoplankton pigments and co-varying associates are the dominant absorbing components. Therefore, the spectral absorption coefficient of pure seawater ( $a_w(\lambda)$ , in  $m^{-1}$ ) may play a vital role in ocean color remote sensing studies in Case 1 waters. This is especially true for the subtropical ocean gyres, which account for approximately 40% of the Earth’s surface area [3] and are reportedly expanding [4]. In addition, the fidelity of  $a_w(\lambda)$  is also essential for better understanding and prediction of in-water penetration of radiation and water transparency in oceanic waters [5,6].

There is a long history in the determination of  $a_w(\lambda)$  [7], and values of  $a_w(\lambda)$  were determined conventionally by laboratory measurements of purified water or estimated from the “clearest” natural water. For brevity, the same term,  $a_w(\lambda)$ , is used herein to represent the “pure water” absorption coefficient obtained from purified water or “clearest” freshwater or seawater. For the ocean color community, the  $a_w(\lambda)$  values from Smith and Baker [8] were generally accepted and used in the 1980’s and 1990’s, which were the upper bound of pure water (seawater) absorption coefficients estimated from the freshwater of Crater Lake, Oregon and the seawater of the Sargasso Sea. Since the 2000’s, the community has adopted the  $a_w(\lambda)$  values of Pope and Fry [9], referred to as  $a_{w\_PF97}$ , as the “standard”, which were determined from carefully prepared “pure water” using an integrating cavity. Recently, new spectral values of  $a_w(\lambda)$  were obtained from

remote sensing reflectance ( $R_{rs}(\lambda)$ , in  $\text{sr}^{-1}$ ) [10], referred to as  $a_w$ \_Lee15, for “pure seawater” based on optical closure in the “clearest” natural waters in the South Pacific Gyre. Moreover, Mason et al. [11] improved the measurements of Pope and Fry [9] using an updated integrating cavity, and their measurements hereafter are referred to as  $a_w$ \_Mason16. It is noted that the two recently obtained  $a_w$ \_Lee15 and  $a_w$ \_Mason16 are lower than  $a_w$ \_PF97 in the blue-green domain (410–550 nm), especially in the blue domain where the differences are about a factor of 2. Given  $a_w(\lambda)$  is a critical input to semi-analytical algorithms for IOPs retrieval, it is logical and necessary to answer the question: what is the impact on the derived IOPs using  $a_w$ \_Lee15 instead of using  $a_w$ \_PF97 that has been adopted for decades?

In this study, a high-quality *in-situ* dataset is first employed to evaluate the validity of  $a_w$ \_PF97 and  $a_w$ \_Lee15 for IOPs retrievals in oligotrophic waters. The impacts of  $a_w(\lambda)$  on the derived IOPs in global oceans are further demonstrated using the Visible Infrared Imaging Radiometer Suite (VIIRS) data, followed by detailed discussions.

## 2. Data and methods

### 2.1. The absorption coefficients of “pure water” and “pure seawater”

Two sets of  $a_w(\lambda)$  data,  $a_w$ \_PF97 and  $a_w$ \_Lee15, are primarily evaluated in this study to demonstrate the impacts of  $a_w(\lambda)$  on the derived IOPs. Values of  $a_w$ \_PF97 were determined from purified water by measuring its absorption and attenuation coefficients using an integrating cavity from 380 to 720 nm, and has been adopted by the ocean color community as a “standard”. Values of  $a_w$ \_Lee15, on the other hand, were inverted from  $R_{rs}(\lambda)$  measured in the South Pacific Gyre for the spectral range between 350 and 550 nm. Specifically,  $R_{rs}(\lambda)$  is a function of the bulk absorption and backscattering coefficients ( $a(\lambda)$  and  $b_b(\lambda)$ , in  $\text{m}^{-1}$ ) [12,13]. With concurrently measured component IOPs and  $R_{rs}(\lambda)$ ,  $a_w$ \_Lee15 was derived analytically from measured  $R_{rs}(\lambda)$  and the absorption coefficients of phytoplankton, suspended particulate matter and colored dissolved organic matter [10]. Note that the values of  $a_w$ \_Lee15 beyond 550 nm were adopted from  $a_w$ \_PF97, as  $a_w(\lambda)$  beyond 550 nm are found very consistent among various determinations [11]. The spectral values of  $a_w$ \_PF97 and  $a_w$ \_Lee15 are illustrated in Fig. 1 to present their differences in the 350–550 nm domain. In addition,  $a_w$ \_Mason16, acknowledged as scattering-independent  $a_w(\lambda)$  measurements of laboratory-grade “pure water” prepared from a sophisticated purification system, is also included in Fig. 1 for comparison. Note that all the three  $a_w(\lambda)$  data were linearly interpolated to 1 nm interval to calculate the differences among two  $a_w(\lambda)$  data, and to obtain  $a_w(\lambda)$  at the VIIRS bands.

### 2.2. In-situ measurements and satellite data

A globally compiled bio-optical *in-situ* dataset [14] was adopted in this study to evaluate the impacts of  $a_w$ \_PF97 and  $a_w$ \_Lee15. Specifically, the distributed  $\pm 2$  nm binned data at VIIRS bands, centered at 410, 443, 486, 551, and 671 nm, respectively, were employed after the following criteria applied:  $R_{rs}(\lambda)$  at the five VIIRS bands and concurrent phytoplankton absorption coefficient ( $a_{ph}(\lambda)$ , in  $\text{m}^{-1}$ ) at 443 nm are available and positive. The spectral quality of  $R_{rs}(\lambda)$  was later checked by the quality assurance score (QA) [15], which ranges between 0 and 1 with 0 stands for questionable data and 1 for perfect quality. In this study, only high-quality  $R_{rs}(\lambda)$  data (QA  $\geq 0.8$ ) were retained for the subsequent analysis. As a result, 736 out of 1004 paired measurements of  $R_{rs}(\lambda)$  and IOPs were used and are hereafter referred to as the Valente\_16 dataset.

Given that the relative contribution of  $a_w(\lambda)$  to  $a(\lambda)$  in the blue-green domain is negligible in coastal waters where the contributions from CDOM and suspended particulates dominate, it is preferred to evaluate the  $a_w(\lambda)$  impacts on the derived IOPs in oligotrophic waters. For oligotrophic waters, such as ocean gyres,  $a(\lambda)$  at 443 nm is typically less than  $0.02 \text{ m}^{-1}$ , as

demonstrated in the global IOPs products distributed by NOAA CoastWatch (figure not shown here). However, the Valente\_16 dataset has no data falling within the range of  $a(443) < 0.02 \text{ m}^{-1}$ . As an alternative, we selected the *in-situ* data with  $a(443) < 0.05 \text{ m}^{-1}$  to represent the oligotrophic water samples in the Valente\_16 dataset and eventually obtained 74 paired measurements in total.

In addition to the *in-situ* dataset, satellite data were also employed to provide a synoptic view of  $a_w(\lambda)$  impacts on the derived IOPs in global oceans. The monthly-binned science-quality VIIRS product of normalized water-leaving radiance ( $nL_w(\lambda)$ , in  $\text{W}/\text{m}^2/\mu\text{m}/\text{sr}$ ), distributed by NOAA CoastWatch, is selected for the demonstration. Specifically, one scene of the monthly-binned product for May 2018 with a spatial resolution of 4 km ('V2018121\_2018151\_D31\_WW00.nc') was downloaded in this effort. The NOAA VIIRS ocean color Level-2 data were processed with the Multi-Sensor Level-1 to Level-2 (MSL12) ocean color data processing system at the NOAA Center for Satellite Applications and Research (STAR). The procedure for monthly-binned Level-3 data is explained in the documents for NOAA ocean color products (Algorithm Theoretical Basis Document (ATBD), version 1.0, June 2017).

### 2.3. IOPs retrieval algorithms

Two well-known semi-analytical algorithms were employed in this study to derive IOPs from  $R_{rs}(\lambda)$ . The first one is the quasi-analytical algorithm (QAA) [16], which is a stepwise algorithm using algebraic equations to solve the absorption and backscattering coefficients of different water components. The latest update (version 6) of QAA, referred to as QAAv6 herein, can be found at [http://www.ioccg.org/groups/Software\\_OCA/QAA\\_v6\\_2014209.pdf](http://www.ioccg.org/groups/Software_OCA/QAA_v6_2014209.pdf). The other algorithm is the generalized IOPs algorithm (GIOP) [17], which derives three eigenvalues that parameterize the spectral absorption coefficients of phytoplankton ( $a_{ph}(\lambda)$ ), colored dissolved organic matter and non-algae particles ( $a_{dg}(\lambda)$ ), and the spectral backscattering coefficients of suspended particles ( $b_{bp}(\lambda)$ ) using spectral optimization. For simplicity, GIOP in this effort employed all default settings, as described in Werdell et al. [17], except for  $a_w(\lambda)$ . The backscattering coefficients of pure seawater ( $b_{bw}(\lambda)$ ) in both QAAv6 and GIOP were adopted from Morel [18].

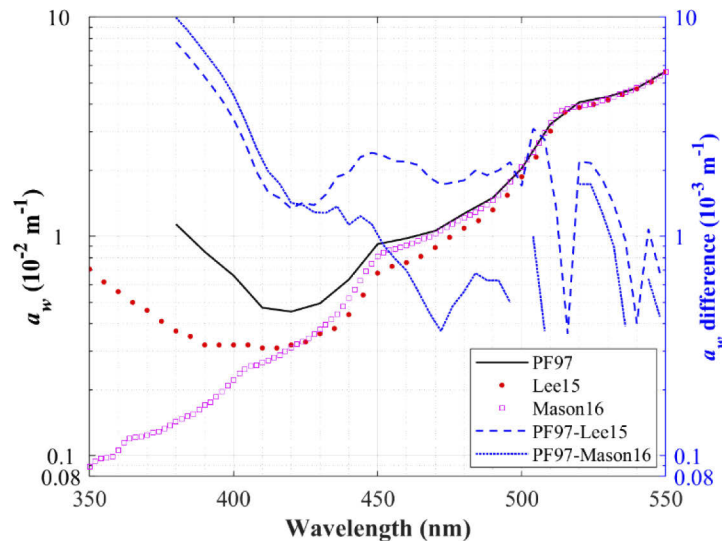


**Fig. 1.** Comparison of three spectral  $a_w(\lambda)$  reported in the literature:  $a_w$ \_PF97 (black line, [9]),  $a_w$ \_Lee15 (red dots, [10]), and  $a_w$ \_Mason16 (magenta squares, [11]). The blue dashed and dotted lines, aligned to the right y-axis, represent the differences between  $a_w$ \_PF97 and that of  $a_w$ \_Lee15 and  $a_w$ \_Mason16, respectively.

Note that the inelastic scattering processes, such as the Raman scattering, also contribute photons to  $R_{rs}(\lambda)$ , especially in the longer wavelengths for oligotrophic waters [19]. Therefore, prior to the implementation of QAAv6 and GIOP, a simple correction on  $R_{rs}(\lambda)$  for the Raman-scattering effect was carried out for the Valente\_16 dataset and the VIIRS data according to Eqs. (11) and (13) of Lee et al. [20].

#### 2.4. Statistical measures

The slope and the coefficient of determination ( $R^2$ ), determined from the Model-II regression [21], and the median absolute percentage difference (MAPD), were calculated to quantitatively evaluate the agreement between the derived IOPs and the measured IOPs. For demonstration with satellite data, the absolute percentage difference (APD) was also introduced to assess the difference in the derived IOPs using the two different  $a_w(\lambda)$ , with the derived IOPs using  $a_w$ \_PF97 as the reference. The MAPD and APD are defined as,

$$\text{MAPD} = \text{Median}(|1 - \text{derived}/\text{measured}| \times 100\%) \quad (1)$$

$$\text{APD} = \frac{|IOP_{Lee15} - IOP_{PF97}|}{IOP_{PF97}} * 100\% \quad (2)$$

where  $IOP_{Lee15}$  and  $IOP_{PF97}$  are the derived IOPs using  $a_w$ \_Lee15 and  $a_w$ \_PF97, respectively.

### 3. Results

#### 3.1. Validations with Valente\_16 dataset

For the oligotrophic water samples in the Valente\_16 dataset, validations of the derived  $a_{ph}(\lambda)$  and  $a_{dg}(\lambda)$  from both GIOP and QAAv6 using  $a_w$ \_Lee15 and  $a_w$ \_PF97, respectively, are shown in Fig. 2. Here examples are presented for the derived IOPs at 410 nm, which is because the

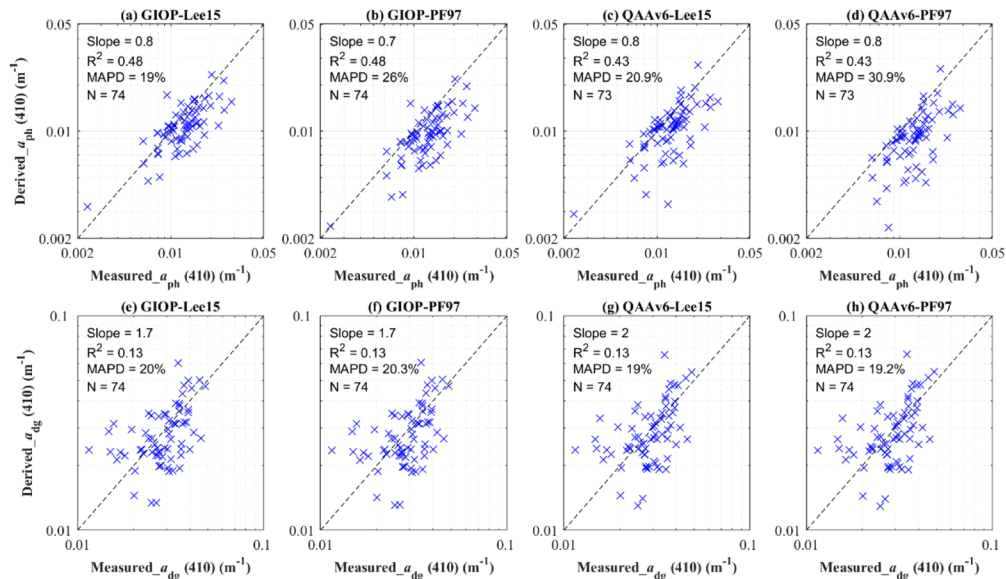


**Fig. 2.** Validation of  $R_{rs}(\lambda)$ -derived  $a_{ph}(410)$  and  $a_{dg}(410)$  from GIOP and QAAv6 and using  $a_w$ \_Lee15 and  $a_w$ \_PF97, respectively, for the oligotrophic subset of the Valente\_16 dataset. The upper and lower panels present the results of the derived  $a_{ph}(410)$  and  $a_{dg}(410)$ , respectively.

relative difference between  $a_{w\_PF97}$  and  $a_{w\_Lee15}$  is the largest at 410 nm for the VIIRS bands (see Fig. 1). A validation of the derived  $b_{bp}(\lambda)$  using the two  $a_w(\lambda)$  could not be done here because no  $b_{bp}(\lambda)$  measurements can be found from the oligotrophic subset of the Valente\_16 dataset.

As shown in Fig. 2, the derived  $a_{ph}(410)$  data using  $a_{w\_Lee15}$  have shown improved agreement with the *in-situ* data compared to the retrievals using  $a_{w\_PF97}$  for both GIOP and QAAv6. Statistically, MAPDs of the derived  $a_{ph}(410)$  using  $a_{w\_Lee15}$  are reduced by 7% and 10% compared to the retrievals using  $a_{w\_PF97}$  for GIOP and QAAv6, respectively. Also, the derived  $a_{ph}(410)$  using  $a_{w\_PF97}$  are systematically underestimated, as shown in Figs. 2(b) and 2(d). In contrast, the derived  $a_{ph}(410)$  using  $a_{w\_Lee15}$  are greater than the retrievals using  $a_{w\_PF97}$  and agree better with the measured  $a_{ph}(410)$  (see Figs. 2(a) and 2(c)), indicating that  $a_{w\_Lee15}$  could be more appropriate to represent the “pure seawater” absorption coefficient and for the retrieval of  $a_{ph}(\lambda)$  in oligotrophic waters. As shown in Figs. 2(e)–2(h), the changes in  $a_w(\lambda)$  only have very small impacts on the derived  $a_{dg}(410)$  for both GIOP and QAAv6, with slightly improved retrievals using  $a_{w\_Lee15}$  than that of using  $a_{w\_PF97}$ .

The  $a_w(\lambda)$  impacts on the derived IOPs at other VIIRS blue bands are further presented in Fig. 3 for the oligotrophic subset of the Valente\_16 dataset. Here only results of the derived  $a_{ph}(\lambda)$  and  $a_{dg}(\lambda)$  at 410, 443, and 486 nm are presented, as the measured  $R_{rs}(\lambda)$  and IOPs at 551 and 671 nm have more uncertainties due to very small values. The  $a_w(\lambda)$  impacts on the derived  $b_{bp}(\lambda)$  will be discussed in Section 3.2 and Section 4.

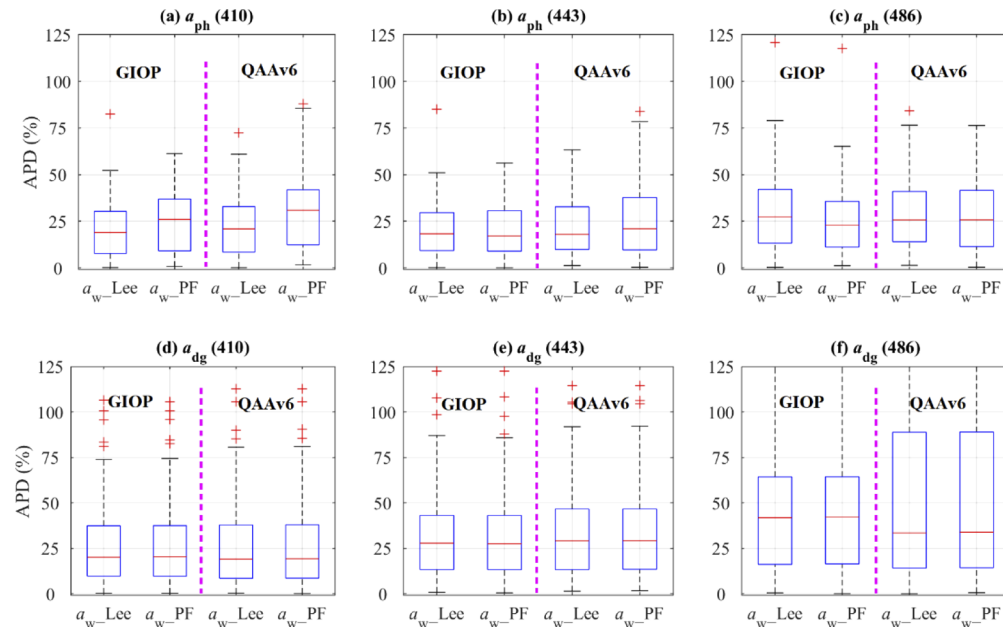


**Fig. 3.** Evaluation of the derived IOPs at three VIIRS bands by GIOP and QAA6 using  $a_{w\_Lee15}$  and  $a_{w\_PF97}$ , respectively. The left two boxes in each subfigure represent the results of GIOP and the right two boxes for QAAv6. The upper and lower panels present the results of the derived  $a_{ph}(\lambda)$  and  $a_{dg}(\lambda)$ , respectively. Calculations of the APDs were based on the same oligotrophic subset used in Fig. 2.

On each box in Fig. 3, the central red mark indicates the MAPD, and the bottom and top edges of the box represent the 25<sup>th</sup> and 75<sup>th</sup> percentiles, respectively. The whiskers extend to the most extreme data points not considered as outliers, and the outliers are plotted individually using the red cross symbol. As shown in Fig. 3, MAPD of the derived  $a_{ph}(\lambda)$  are overall smaller for

the retrievals using  $a_w$ \_Lee15 for both GIOP and QAAv6 (see Figs. 3(a)–3(c)), suggesting that more accurate retrievals of  $a_{ph}(\lambda)$  are obtained when  $a_w$ \_Lee15 is employed. Further, as shown in Figs. 3(d)–3(f), it appears that the selection of different  $a_w(\lambda)$  data has minimal impacts on the derived  $a_{dg}(\lambda)$  for both GIOP and QAAv6, as MAPD of the derived  $a_{dg}(\lambda)$  using the two  $a_w(\lambda)$  are quite comparable. The minimal impacts of  $a_w(\lambda)$  selection on the derived  $a_{dg}(\lambda)$  can be well explained by the spectral feature of the difference between  $a_w$ \_Lee15 and  $a_w$ \_PF97 in the blue domain.

For QAAv6,  $a_w(\lambda)$  are primarily employed in the steps to decompose the algebraically solved  $a(\lambda)$  into  $a_{dg}(\lambda)$  and  $a_{ph}(\lambda)$ . Because the differences between  $a_w$ \_PF97 and  $a_w$ \_Lee15 in the ~410–470 nm domain have a spectral pattern that matches the spectral feature of  $a_{ph}(\lambda)$  (see the blue dashed line in Fig. 1), the use of  $a_w$ \_Lee15 rather than  $a_w$ \_PF97 will have more impacts on the derived  $a_{ph}(\lambda)$ , instead of  $a_{dg}(\lambda)$ . In other words, the difference in using  $a_w$ \_Lee15 rather than using  $a_w$ \_PF97 is well compensated by a change of  $a_{ph}(\lambda)$ . Moreover, QAAv6-derived  $b_{bp}(\lambda)$  are only affected by the difference between  $a_w$ \_PF97 and  $a_w$ \_Lee15 at 550 nm (see Table 2 of Lee et al. [16]), which is, however, only about 0.53%. Therefore, using  $a_w$ \_PF97 or  $a_w$ \_Lee15 will have limited impacts on the derived  $b_{bp}(\lambda)$ .

For GIOP, however, changes in  $a_w(\lambda)$  will generally be propagated to all three eigenvalues due to the use of spectral optimization with all available  $R_{rs}(\lambda)$  in the visible domain as the input. Again, because the differences between  $a_w$ \_PF97 and  $a_w$ \_Lee15 in the blue domain have a similar spectral pattern to  $a_{ph}(\lambda)$ , and that  $a_{ph}(\lambda)$  and  $a_{dg}(\lambda)$  do not contribute much to the total absorption in the green band for oligotrophic waters, the differences between  $a_w$ \_PF97 and  $a_w$ \_Lee15 are generally compensated by the changes of  $a_{ph}(\lambda)$ , rather than the changes of  $a_{dg}(\lambda)$  and  $b_{bp}(\lambda)$ .

### 3.2. Demonstrations with VIIRS data

Validation with the *in-situ* dataset shows that  $a_w$ \_Lee15 could be more appropriate for IOPs retrievals in oligotrophic waters. Here, NOAA VIIRS monthly-binned data are employed to compare the retrieved IOPs of global waters using the two spectral  $a_w(\lambda)$  and to demonstrate the impacts of  $a_w(\lambda)$ . Figure 4 shows the comparisons of derived  $a_{ph}(443)$  using  $a_w$ \_Lee15 and  $a_w$ \_PF97 for the two inversion algorithms.

**Table 1. The range (minimum - maximum) of derived IOPs and APD for the selected oligotrophic core zone in the North Atlantic Gyre, as highlighted in Fig. 4(e). The number in the brackets implies the median value.**

		Lee15 ( $10^{-3} \text{ m}^{-1}$ )	PF97 ( $10^{-3} \text{ m}^{-1}$ )	APD (%)
GIOP	$a_{ph}(443)$	2.9 - 6.5 (4.0)	1.4 - 5.0 (2.5)	30.1 - 145.5 (59.2)
	$a_{dg}(443)$	3.5 - 5.9 (4.1)	3.2 - 5.7 (3.9)	3.7 - 9.5 (6.6)
	$b_{bp}(443)$	0.5 - 1.5 (1.0)	0.6 - 1.6 (1.1)	5.5 - 11.1 (7.3)
QAAv6	$a_{ph}(443)$	2.7 - 7.7 (4.8)	0.8 - 5.8 (2.8)	33.4 - 237.6 (68.2)
	$a_{dg}(443)$	4.0 - 7.1 (5.0)	3.9 - 7.0 (5.0)	0.9 - 2.1 (1.5)
	$b_{bp}(443)$	0.6 - 2.1 (1.4)	0.6 - 2.1 (1.4)	0.7 - 1.4 (0.9)

As shown in Figs. 4(a)–4(d), the primary differences between the derived  $a_{ph}(443)$  using the two  $a_w(\lambda)$  are observed in oligotrophic waters, such as the ocean gyres, where the derived  $a_{ph}(443)$  using  $a_w$ \_Lee15 are much higher than the retrievals using  $a_w$ \_PF97. As explicitly shown in Figs. 4(e) and 4(f), APD of the derived  $a_{ph}(443)$  using the two sets of  $a_w(\lambda)$  is found over 30% in the ocean gyres and increases rapidly towards the gyres' core. For instance, in the oligotrophic core zone of the North Atlantic Gyre (hereafter referred to as cNAG), defined according to Morel et al. [22] and highlighted in Figs. 4(e) and 4(f), the derived  $a_{ph}(443)$  using  $a_w$ \_Lee15 are up to 146% and 238% larger than that of using  $a_w$ \_PF97 for GIOP and QAAv6, respectively. Detailed

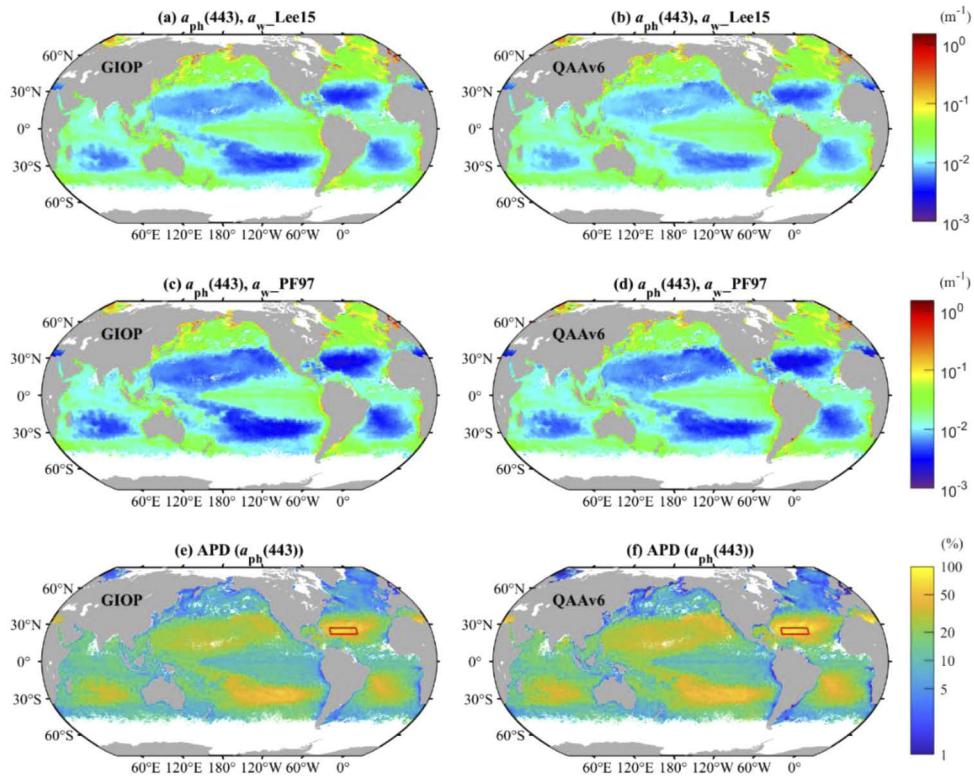


**Fig. 4.** Global distribution of derived  $a_{ph}(443)$  from VIIRS data using  $a_{w\_Lee15}$  and  $a_{w\_PF97}$  and the absolute percentage difference between the two derived  $a_{ph}(443)$ . The left panel presents the results from GIOP while the right panel for QAAv6. The red box superimposed on panels (e) and (f) highlights the oligotrophic core zone in the North Atlantic Gyre, defined by Morel et al. [22], for statistical analysis in Table 1.

statistical results regarding the derived component IOPs within cNAG are tabulated in Table 1. Also, consistent with the validation results with the Valente\_16 dataset,  $a_w(\lambda)$  impacts on the derived  $a_{ph}(443)$  are less significant for GIOP, where a smaller median APD of 59.2% is found compared to the median APD of 68.2% for QAAv6. Moreover, as shown in Figs. 4(e) and 4(f), for optically complex waters, such as most coastal waters,  $a_w(\lambda)$  impacts on the derived  $a_{ph}(443)$  for both GIOP and QAAv6 can be neglected given that the APD is generally less than 2%.

Comparisons of the derived  $a_{ph}(\lambda)$  at other VIIRS bands are not shown here for brevity, but  $a_w(\lambda)$  impacts on the derived  $a_{ph}(\lambda)$  at other wavelengths are deducible. For QAAv6,  $a_w(\lambda)$  impacts on the derived  $a_{ph}(\lambda)$  are wavelength-dependent, which are determined by both the difference between  $a_{w\_Lee15}$  and  $a_{w\_PF97}$  and the magnitude of the derived  $a_{ph}(\lambda)$  at the specific wavelength. The impacts of  $a_w(\lambda)$  on the derived  $a_{ph}(\lambda)$  beyond 550 nm would be negligible. For GIOP, on the other hand,  $a_w(\lambda)$  impacts on the derived  $a_{ph}(\lambda)$  would be wavelength-independent, as it is a scaling of the pre-determined spectral shape of  $a_{ph}(\lambda)$ .

Demonstrations for QAAv6-derived global  $a_{dg}(\lambda)$  and  $b_{bp}(\lambda)$  are not presented here, as the impacts of  $a_w(\lambda)$  (between  $a_{w\_Lee15}$  and  $a_{w\_PF97}$ ) on QAAv6-derived  $a_{dg}(\lambda)$  and  $b_{bp}(\lambda)$  are expected to be relatively small (see Fig. 2 and Fig. 3). As tabulated in Table 1, the median APD of QAAv6-derived  $a_{dg}(443)$  and  $b_{bp}(443)$  within cNAG are only 1.5% and 0.9%, respectively. Moreover, because  $a_{dg}(\lambda)$  and  $b_{bp}(\lambda)$  are based on spectral models in QAAv6, the impacts of  $a_w(\lambda)$  on QAAv6-derived  $a_{dg}(\lambda)$  and  $b_{bp}(\lambda)$  would be wavelength-independent.

The impacts of  $a_w(\lambda)$  on GIOP-derived  $a_{dg}(\lambda)$  and  $b_{bp}(\lambda)$  are further evaluated, and demonstrations for the derived  $a_{dg}(\lambda)$  and  $b_{bp}(\lambda)$  at 443 nm are presented in Fig. 5 as an example. As expected, the differences between  $a_{w\_Lee15}$  and  $a_{w\_PF97}$  also result in discrepancies in the derived  $a_{dg}(\lambda)$  and  $b_{bp}(\lambda)$ , but the impacts are much less significant than that of the derived  $a_{ph}(\lambda)$ , with APDs of  $a_{dg}(443)$  and  $b_{bp}(443)$  are generally less than 10% for the ocean gyres (see Figs. 5(e) and 5(f)). Specifically, for the cNAG, the median APDs for GIOP-derived  $a_{dg}(443)$  and  $b_{bp}(443)$  are 6.6% and 7.3%, respectively (see Table 1 for details). In the non-oligotrophic waters,  $a_w(\lambda)$  impacts on GIOP-derived  $a_{dg}(\lambda)$  and  $b_{bp}(\lambda)$  are negligible with APD generally less than 1% (see Figs. 5(e) and 5(f)).

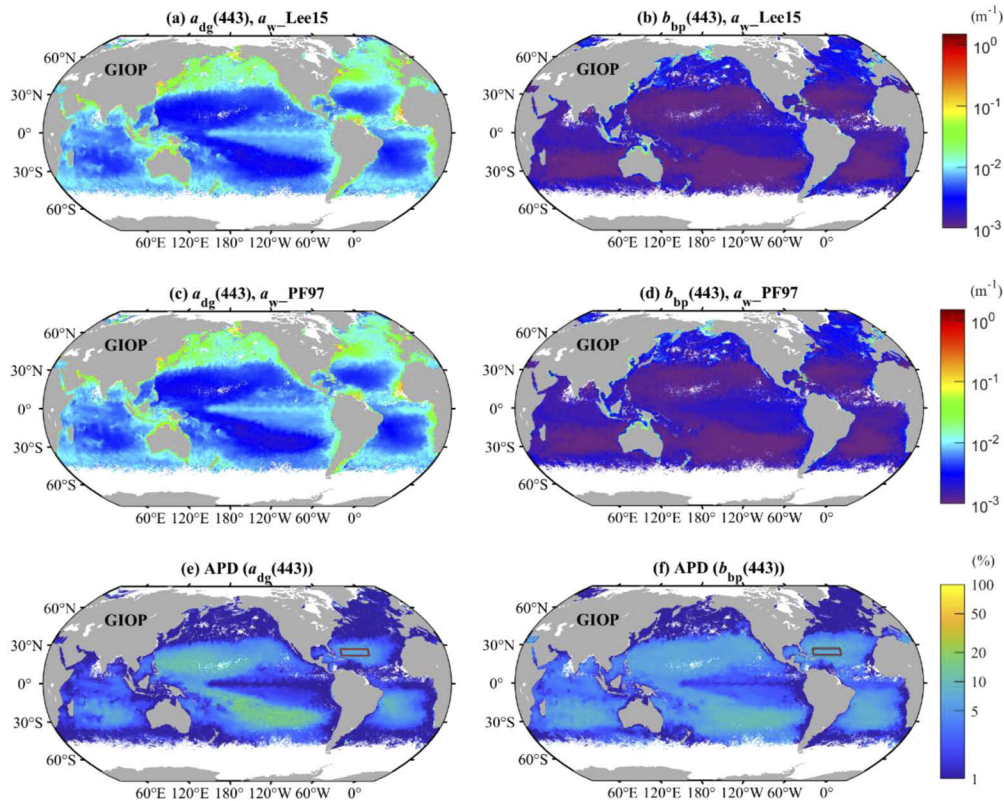


**Fig. 5.** Same as Fig. 4, but for GIOP-derived  $a_{dg}(443)$  and  $b_{bp}(443)$ . The left panel presents the results for  $a_{dg}(443)$  and the right panel for  $b_{bp}(443)$ .

#### 4. Discussion and conclusions

Lee et al. [10] argued that  $a_{w\_PF97}$  could be less reliable than  $a_{w\_Lee15}$  in oligotrophic waters from indirect validation results, as using  $a_{w\_PF97}$  resulted in negative retrievals of  $a_{ph}(488)$  and a wider range of  $a_{ph}(488)/a_{ph}(443)$  that was inconsistent with field measurements. The present validation results with the Valente\_16 dataset confirm that  $a_{w\_Lee15}$  is more appropriate for IOPs retrievals in oligotrophic waters. This could be explained by the uncertainties of  $a_{w\_PF97}$  in the ultraviolet-blue domain due to several limitations in the measurement, such as difficulties in preparing laboratory-grade “pure water”, inadequate instrument sensitivity for low absorption measurements, and insufficient correction of the scattering effects. In addition, the integrating

cavity used in Pope and Fry [9] was made of the diffuse reflecting material Spectralon, which could absorb light between 380 and 440 nm [11].

The questionable quality of  $a_w$ \_PF97 within the blue-green domain is also confirmed when comparing it with  $a_w$ \_Mason16 (see Fig. 1), which is considered to be of higher accuracy as the aforementioned issues in the  $a_w$ \_PF97 measurement have been largely addressed with more advanced instrumentation. Demonstration for the impacts of using  $a_w$ \_Mason16 on the derived IOPs at the global scale is not presented in this study, but the derived IOPs using  $a_w$ \_Mason16 could be deduced. The  $a_w(\lambda)$  impacts on the derived IOPs in oligotrophic waters depend mainly on the spectral pattern of the difference between the two  $a_w(\lambda)$  data. As shown in Fig. 1, the spectral pattern of the difference between  $a_w$ \_PF97 and  $a_w$ \_Mason16 (see the blue dotted line in Fig. 1) is similar to that of  $a_{dg}(\lambda)$ . Therefore, the use of  $a_w$ \_Mason16 will likely have more impacts on the derived  $a_{dg}(\lambda)$ , rather than  $a_{ph}(\lambda)$ . Here we compared the impacts of using  $a_w$ \_Mason16 and  $a_w$ \_Lee15 on the derived IOPs, with retrievals using  $a_w$ \_PF97 as the reference, and presented the results in Fig. 6 with the derived IOPs at 410 nm as the example. As shown in Fig. 6, compared to the use of  $a_w$ \_PF97, a use of  $a_w$ \_Mason16 will result in a significant difference in the derived  $a_{dg}(410)$ , while at the same time, quite small differences in the derived  $a_{ph}(\lambda)$  and  $b_{bp}(\lambda)$ . This pattern of impact is opposite to the use of  $a_w$ \_Lee15. In other words, a use of  $a_w$ \_Mason16 will not improve much on the retrieval of  $a_{ph}(\lambda)$  in oligotrophic waters; on the other hand, a use of  $a_w$ \_Mason16 will negatively impact the retrieval of  $a_{dg}(\lambda)$  in oligotrophic waters (MAPD increased from 19.2% to 21.8% for QAAv6-derived  $a_{dg}(\lambda)$  for the oligotrophic subset of the Valente\_16 dataset, figure not shown here).

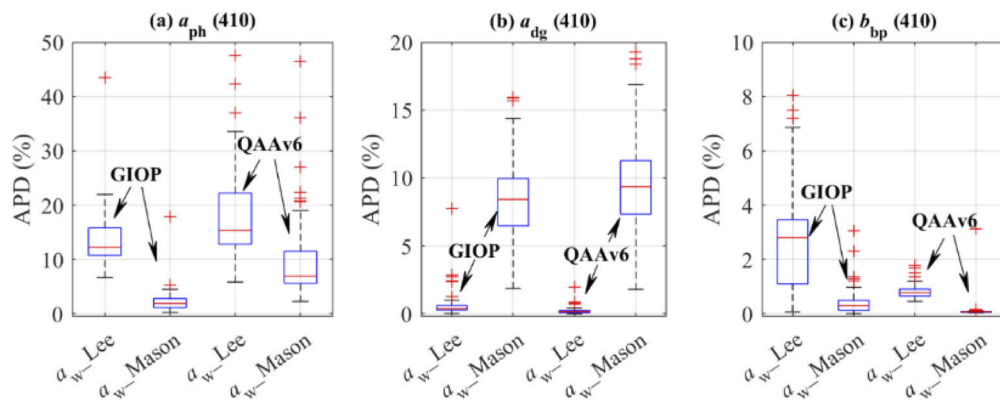


**Fig. 6.** The impacts of  $a_w$ \_Mason16 on the derived IOPs at 410 nm compared to that of using  $a_w$ \_Lee15. Note that the derived IOPs using  $a_w$ \_PF97 were used as the reference to calculate the APD, and the same oligotrophic subset used in Fig. 2 was employed here.

Again, there is not a significant impact on the retrieval of  $b_{bp}(\lambda)$  (see Fig. 6(c)) when  $a_w$ \_Mason16 is used, which is because  $b_{bp}$  is primarily determined from  $R_{rs}$  in the longer wavelengths where the absorption coefficient of pure seawater plays a major role [23]. Therefore, the retrieved  $b_{bp}(\lambda)$  by both QAAv6 and GIOP will be less sensitive to the changes of  $a_w(\lambda)$  in the blue.

Further, it is necessary to point out that  $a_w$ \_Lee15 represents the absorption coefficient of “pure seawater”, while  $a_w$ \_Mason16 represents the absorption coefficient of “pure water”. The significant divergences between  $a_w$ \_Lee15 and  $a_w$ \_Mason16 for  $\lambda < \sim 410$  nm are likely due to the impact of sea salts [11]. Thus,  $a_w$ \_Lee15 might be more appropriate for applications of oceanic waters, especially the use of  $a_w$ \_Mason16 will not improve the retrieval of  $a_{ph}(\lambda)$  in oligotrophic waters (see Fig. 6(a)). Also, note that there will be more measurements or sensors that are capable of measuring  $R_{rs}(\lambda)$  in the 350–410 nm domain, such as the Ocean and Land

Colour Instrument (OLCI) and the forthcoming Plankton, Aerosol, Cloud, ocean Ecosystem (PACE) mission, thus a validation of  $a_w$ \_Lee15 in the 350–410 nm domain demands more field measurements in the ocean gyres.

Assuming the derived IOPs using  $a_w$ \_Lee15 are closer to the “true” IOPs in natural oceanic waters, the demonstrations here with the VIIRS data indicate larger uncertainties of the derived IOPs using  $a_w$ \_PF97 in oligotrophic waters, especially for the derived  $a_{ph}(\lambda)$ . Note that  $a_w$ \_PF97 has been accepted as the “standard”  $a_w(\lambda)$  in the past two decades, the uncertainty of  $a_w$ \_PF97 will be propagated not only to the derived IOPs but also to the IOPs derivative products. Due to the comprehensive observation by ocean color satellites, remotely sensed IOPs had been widely used in interdisciplinary studies to investigate ocean biological processes and global biogeochemical cycles [24,25]. For instance, the values of  $a_{ph}(\lambda)$  were adopted in estimating the primary production [26], phytoplankton pigment concentrations [27], and phytoplankton size spectrum and size classes [28,29]. The significant underestimation of the derived  $a_{ph}(\lambda)$  using  $a_w$ \_PF97 would introduce uncertainties to these derivative products, especially for applications in oligotrophic waters. Take the estimation of primary production for example, when it uses  $a_{ph}(443)$  to scale up [26], the estimated primary production in cNAG could be up to 248% lower if  $a_w$ \_PF97 is employed to derive  $a_{ph}(443)$  instead of  $a_w$ \_Lee15.

More importantly, although the  $a_w(\lambda)$  impacts on the derived IOPs are only evaluated for QAA and GIOP in this study, it is reasonable to assume that  $a_w(\lambda)$  may have similar impacts on the derived component IOPs of oligotrophic waters for other semi-analytical inversion algorithms [30–32]. This is mainly because  $R_{rs}(\lambda)$  is a function of bulk absorption and backscattering coefficients, the changes in  $a_w(\lambda)$  will be inevitably compensated by the derived IOPs of other components when a semi-analytical algorithm is applied.

To conclude, this study shows that the commonly accepted  $a_w$ \_PF97 by the ocean color community could introduce large uncertainties in remotely sensed IOPs in oligotrophic waters, especially for  $a_{ph}(\lambda)$ . Therefore, it is important for the community to adopt a more appropriate spectral  $a_w(\lambda)$  in the practices of IOPs retrievals at global scales, and  $a_w$ \_Lee15 is recommended before more convincing  $a_w(\lambda)$  data become available for “pure seawater”.

## Funding

National Natural Science Foundation of China (41830102, 41890803); Ministry of Science and Technology of the People’s Republic of China (2016YFA0601201, 2016YFC1400905); State Key Laboratory of Marine Environmental Science (2019356).

## Acknowledgments

This work was supported by the NSFC (#41890803 and #41830102), the Chinese Ministry of Science and Technology through the National Key Research and Development Program of China (#2016YFA0601201 and #2016YFC1400905), the Outstanding Postdoctoral Scholarship of the State Key Laboratory of Marine Environmental Science at Xiamen University (Contribution No. 2019356), and the Joint Polar Satellite System (JPSS) funding for the NOAA ocean color calibration and validation (Cal/Val) project. We thank two anonymous reviewers for their constructive comments.

## References

1. C. D. Mobley, “*Light and water : radiative transfer in natural waters*,” Academic press (1994).
2. A. Morel, “Optical Modeling of the Upper Ocean in Relation to Its Biogenous Matter Content (Case-I Waters),” *J. Geophys. Res.* **93**(C9), 10749–10768 (1988).
3. C. R. McClain, S. R. Signorini, and J. R. Christian, “Subtropical gyre variability observed by ocean-color satellites,” *Deep Sea Res., Part II* **51**(1-3), 281–301 (2004).
4. J. J. Polovina, E. A. Howell, and M. Abecassis, “Ocean’s least productive waters are expanding,” *Geophys. Res. Lett.* **35**(3), L03618 (2008).

5. A. P. Vasilkov, J. R. Herman, Z. Ahmad, M. Kahru, and B. G. Mitchell, "Assessment of the ultraviolet radiation field in ocean waters from space-based measurements and full radiative-transfer calculations," *Appl. Opt.* **44**(14), 2863–2869 (2005).
6. A. Morel, B. Gentili, H. Claustre, M. Babin, A. Bricaud, J. Ras, and F. Tieche, "Optical properties of the "clearest" natural waters," *Limnol. Oceanogr.* **52**(1), 217–229 (2007).
7. M. Fewell and A. von Trojan, "Absorption of light by water in the region of high transparency: recommended values for photon-transport calculations," *Appl. Opt.* **58**(9), 2408–2421 (2019).
8. R. C. Smith and K. S. Baker, "Optical properties of the clearest natural waters (200–800 nm)," *Appl. Opt.* **20**(2), 177–184 (1981).
9. R. M. Pope and E. S. Fry, "Absorption spectrum (380–700 nm) of pure water. II. Integrating cavity measurements," *Appl. Opt.* **36**(33), 8710–8723 (1997).
10. Z. Lee, J. Wei, K. Voss, M. Lewis, A. Bricaud, and Y. Huot, "Hyperspectral absorption coefficient of "pure" seawater in the range of 350–550 nm inverted from remote sensing reflectance," *Appl. Opt.* **54**(3), 546–558 (2015).
11. J. D. Mason, M. T. Cone, and E. S. Fry, "Ultraviolet (250–550 nm) absorption spectrum of pure water," *Appl. Opt.* **55**(25), 7163–7172 (2016).
12. H. R. Gordon, O. B. Brown, R. H. Evans, J. W. Brown, R. C. Smith, K. S. Baker, and D. K. Clark, "A Semianalytic Radiance Model of Ocean Color," *J. Geophys. Res.* **93**(D9), 10909–10924 (1988).
13. Z. Lee, K. Du, K. J. Voss, G. Zibordi, B. Lubac, R. Arnone, and A. Weidemann, "An inherent-optical-property-centered approach to correct the angular effects in water-leaving radiance," *Appl. Opt.* **50**(19), 3155–3167 (2011).
14. A. Valente, S. Sathyendranath, V. Brotas, S. Groom, M. Grant, M. Taberner, D. Antoine, R. Arnone, W. M. Balch, and K. Barker, "A compilation of global bio-optical in situ data for ocean-colour satellite applications," *Earth Syst. Sci. Data* **8**(1), 235–252 (2016).
15. J. Wei, Z. Lee, and S. Shang, "A system to measure the data quality of spectral remote-sensing reflectance of aquatic environments," *J. Geophys. Res.* **121**(11), 8189–8207 (2016).
16. Z. Lee, K. L. Carder, and R. A. Arnone, "Deriving inherent optical properties from water color: a multiband quasi-analytical algorithm for optically deep waters," *Appl. Opt.* **41**(27), 5755–5772 (2002).
17. P. J. Werdell, B. A. Franz, S. W. Bailey, G. C. Feldman, E. Boss, V. E. Brando, M. Dowell, T. Hirata, S. J. Lavender, and Z. Lee, "Generalized ocean color inversion model for retrieving marine inherent optical properties," *Appl. Opt.* **52**(10), 2019–2037 (2013).
18. A. Morel, "Optical properties of pure water and pure sea water," *Proc. SPIE* **2258**, 174–183 (1974).
19. H. R. Gordon, "Influence of Raman scattering on the light field in natural waters: a simple assessment," *Opt. Express* **22**(3), 3675–3683 (2014).
20. Z. Lee, C. Hu, S. Shang, K. Du, M. Lewis, R. Arnone, and R. Brewin, "Penetration of UV-visible solar radiation in the global oceans: Insights from ocean color remote sensing," *J. Geophys. Res.* **118**(9), 4241–4255 (2013).
21. E. A. Laws, *Mathematical methods for oceanographers: An introduction*, John Wiley & Sons (1997).
22. A. Morel, H. Claustre, and B. Gentili, "The most oligotrophic subtropical zones of the global ocean: similarities and differences in terms of chlorophyll and yellow substance," *Biogeosciences* **7**(10), 3139–3151 (2010).
23. Z. Lee, S. Shang, Y. Wang, J. Wei, and J. Ishizaka, "Nature of optical products inverted semianalytically from remote sensing reflectance of stratified waters," *Limnol. Oceanogr.* (2019). doi: 10.1002/lno.11307.
24. D. A. Siegel, M. Behrenfeld, S. Maritorea, C. R. McClain, D. Antoine, S. W. Bailey, P. S. Bontempi, E. S. Boss, H. M. Dierssen, S. C. Doney, R. E. Eplee, R. H. Evans, G. C. Feldman, E. Fields, B. A. Franz, N. A. Kuring, C. Mengelt, N. B. Nelson, F. S. Patt, W. D. Robinson, J. L. Sarmiento, C. M. Swan, P. J. Werdell, T. K. Westberry, J. G. Wilding, and J. A. Yoder, "Regional to global assessments of phytoplankton dynamics from the SeaWiFS mission," *Remote Sens. Environ.* **135**, 77–91 (2013).
25. H. M. Dierssen, "Perspectives on empirical approaches for ocean color remote sensing of chlorophyll in a changing climate," *Proc. Natl. Acad. Sci. U. S. A.* **107**(40), 17073–17078 (2010).
26. Z. Lee, J. Marra, M. J. Perry, and M. Kahru, "Estimating oceanic primary productivity from ocean color remote sensing: A strategic assessment," *J. Mar. Syst.* **149**, 50–59 (2015).
27. J. R. Moisan, T. A. H. Moisan, and M. A. Linkswiler, "An inverse modeling approach to estimating phytoplankton pigment concentrations from phytoplankton absorption spectra," *J. Geophys. Res.* **116**(C9), C09018 (2011).
28. T. Hirata, J. Aiken, N. Hardman-Mountford, T. J. Smyth, and R. G. Barlow, "An absorption model to determine phytoplankton size classes from satellite ocean colour," *Remote Sens. Environ.* **112**(6), 3153–3159 (2008).
29. S. Roy, S. Sathyendranath, H. Bouman, and T. Platt, "The global distribution of phytoplankton size spectrum and size classes from their light-absorption spectra derived from satellite data," *Remote Sens. Environ.* **139**, 185–197 (2013).
30. IOCCG, "Remote Sensing of Inherent Optical Properties: Fundamentals, Tests of Algorithms, and Applications," Z. P. Lee (ed.), Reports of the International Ocean-Colour Coordinating Group **No. 5**, IOCCG, Dartmouth, Canada (2006).
31. X. Yu, M. S. Salama, F. Shen, and W. Verhoef, "Retrieval of the diffuse attenuation coefficient from GOCI images using the 2SeaColor model: A case study in the Yangtze Estuary," *Remote Sens. Environ.* **175**, 109–119 (2016).
32. F. E. Hoge, C. W. Wright, P. E. Lyon, R. N. Swift, and J. K. Yungel, "Satellite retrieval of inherent optical properties by inversion of an oceanic radiance model: a preliminary algorithm," *Appl. Opt.* **38**(3), 495–504 (1999).